

## Electronic Supplementary Information

### Precise control of density and strength of acid sites of MFI-type zeolite nanoparticles via simultaneous isomorphous substitution by Al and Fe

Mizuho Yabushita,<sup>\*,†,a</sup> Hiroki Kobayashi,<sup>a</sup> Atsushi Neya,<sup>a</sup> Masafumi Nakaya,<sup>a</sup> Sachiko Maki,<sup>a</sup>  
Masaki Matsubara,<sup>a,b</sup> Kiyoshi Kanie<sup>a</sup> and Atsushi Muramatsu<sup>\*,a,c</sup>

<sup>a</sup>*Institute of Multidisciplinary Research for Advanced Materials, Tohoku University, 2-1-1 Katahira, Aoba-ku, Sendai, Miyagi 980-8577, Japan*

<sup>b</sup>*National Institute of Technology, Sendai College, 48 Nodayama, Medeshima-Shiote, Natori, Miyagi 981-1239, Japan*

<sup>c</sup>*Core Research for Evolutional Science and Technology, Japan Science and Technology Agency, 4-1-8 Honcho, Kawaguchi, Saitama 332-0012, Japan*

*\*Corresponding authors: m.yabushita@tohoku.ac.jp (M.Y.); mura@tohoku.ac.jp (A.M.)*

*†Present address: Department of Applied Chemistry, School of Engineering, Tohoku University, Aoba 6-6-07, Aramaki, Aoba-ku, Sendai, Miyagi 980-8579, Japan*

## Table of Contents

1. Fig. S1	N <sub>2</sub> physisorption isotherms of the synthesized MFI zeolites. ....	S3
2. Fig. S2	Parametric plot of external surface area determined by the <i>t</i> -plot method as a function of the crystallite size.....	S4
3. Fig. S3	<sup>27</sup> Al MAS NMR spectra of the synthesized MFI zeolites. ....	S5
4. Fig. S4	NH <sub>3</sub> -TPD profiles of the synthesized MFI zeolites.....	S6
5. Fig. S5	Parametric plot of apparent $\Delta H_{\text{NH}_3}$ for a physical mixture of A50F0 and A0F50 at the different mixing ratios as a function of the proportion of Al in the total amount of Al and Fe. ....	S7
6. Fig. S6	DRIFT spectra of the [Al, Fe]-MFI zeolites.....	S7
7. Fig. S7	Detailed data of the DTO reaction using A50F0. ....	S8
8. Fig. S8	Detailed data of the DTO reaction using A100F0. ....	S8
9. Fig. S9	Detailed data of the DTO reaction using A200F0. ....	S9
10. Fig. S10	Detailed data of the DTO reaction using A400F0. ....	S9
11. Fig. S11	Detailed data of the DTO reaction using A0F50. ....	S10
12. Fig. S12	Detailed data of the DTO reaction using A0F100. ....	S10
13. Fig. S13	Detailed data of the DTO reaction using A50F50. ....	S11
14. Fig. S14	Detailed data of the DTO reaction using A100F50. ....	S11
15. Fig. S15	Detailed data of the DTO reaction using A200F50. ....	S12
16. Fig. S16	Detailed data of the DTO reaction using A400F50. ....	S12
17. Fig. S17	Detailed data of the DTO reaction using A800F50. ....	S13
18. Fig. S18	Detailed data of the DTO reaction using A100F100. ....	S13
19. Fig. S19	Detailed data of the DTO reaction using A150F75. ....	S14
20. Fig. S20	Detailed data of the DTO reaction using A300F150. ....	S14
21. Table S1	Ratios of propene to ethene produced in the DTO reaction .....	S15
22. Table S2	Reported catalysts for the DTO reactions.....	S16
23. Fig. S21	Differences of catalyst lifetime in the DTO reactions between [Al, Fe]-MFI and a physical mixture of A50F0 and A0F50 at the various Al/(Al + Fe) values. ....	S17
24. Fig. S22	Recycle test of A200F50 for the DTO reaction.....	S17
25. Fig. S23	Detailed data of the second run of the DTO reaction using A200F50. ....	S18
26. Fig. S24	Detailed data of the third run of the DTO reaction using A200F50. ....	S18
27. Fig. S25	Differences of the nature of Fe species involved in the fresh A200F50 catalyst and the one after the third run of recycle test. ....	S19
28. Supplementary references .....		S19

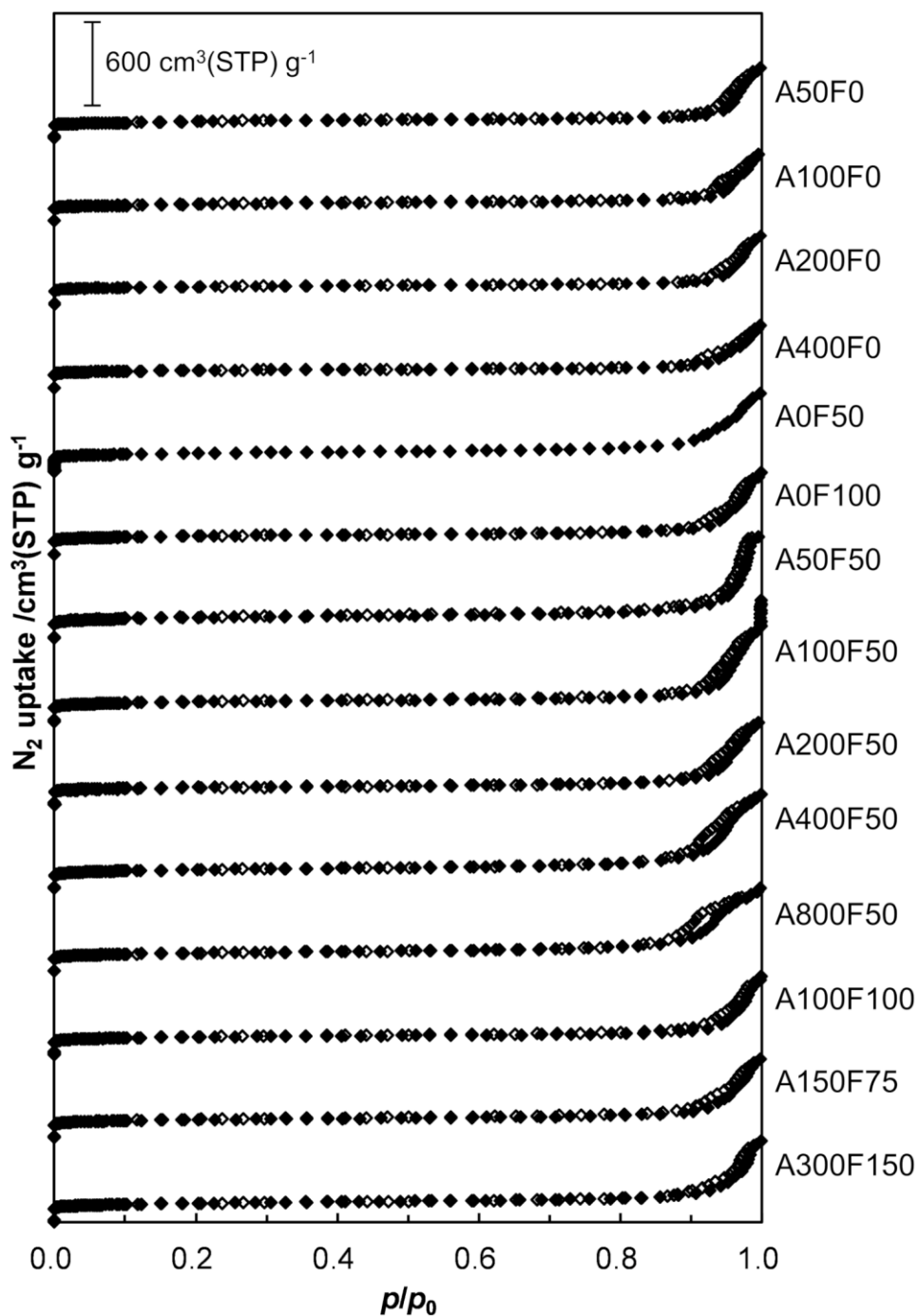


**Fig. S1**  $N_2$  physisorption isotherms of the synthesized MFI zeolites, recorded at  $-196\text{ }^\circ\text{C}$ . For ease of viewing, each isotherm has been shifted vertically. Closed dots show the adsorption branches and open dots represent the desorption branches.

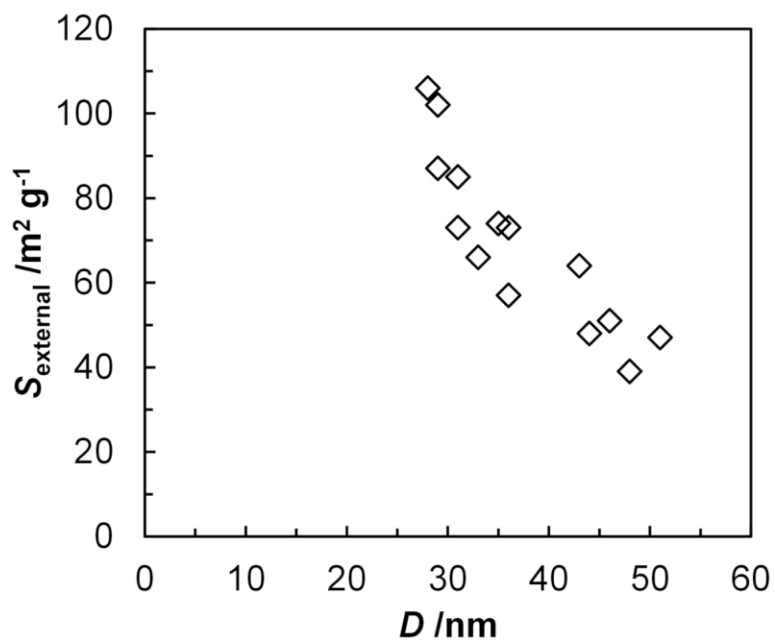


**Fig. S2** Parametric plot of external surface area determined by the  $t$ -plot method ( $S_{\text{external}}$ ) as a function of the crystallite size ( $D$ ).

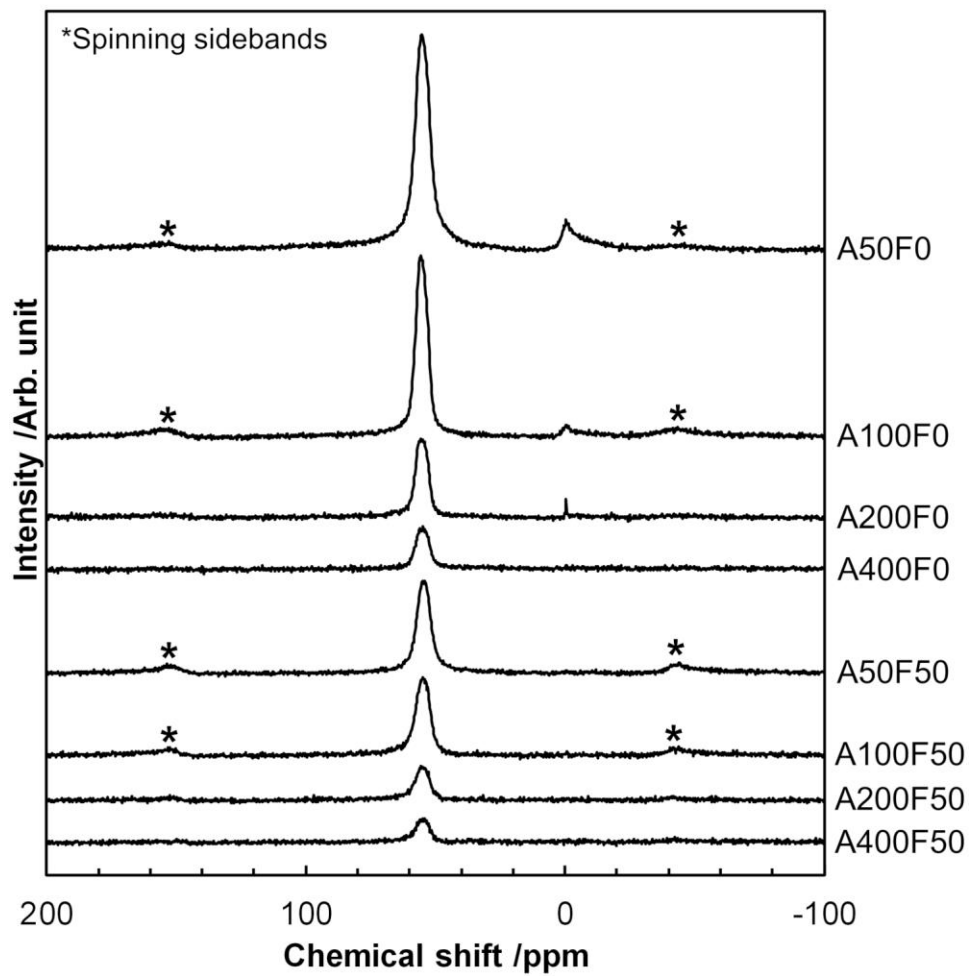


**Fig. S3**  $^{27}\text{Al}$  MAS NMR spectra of the synthesized MFI zeolites.

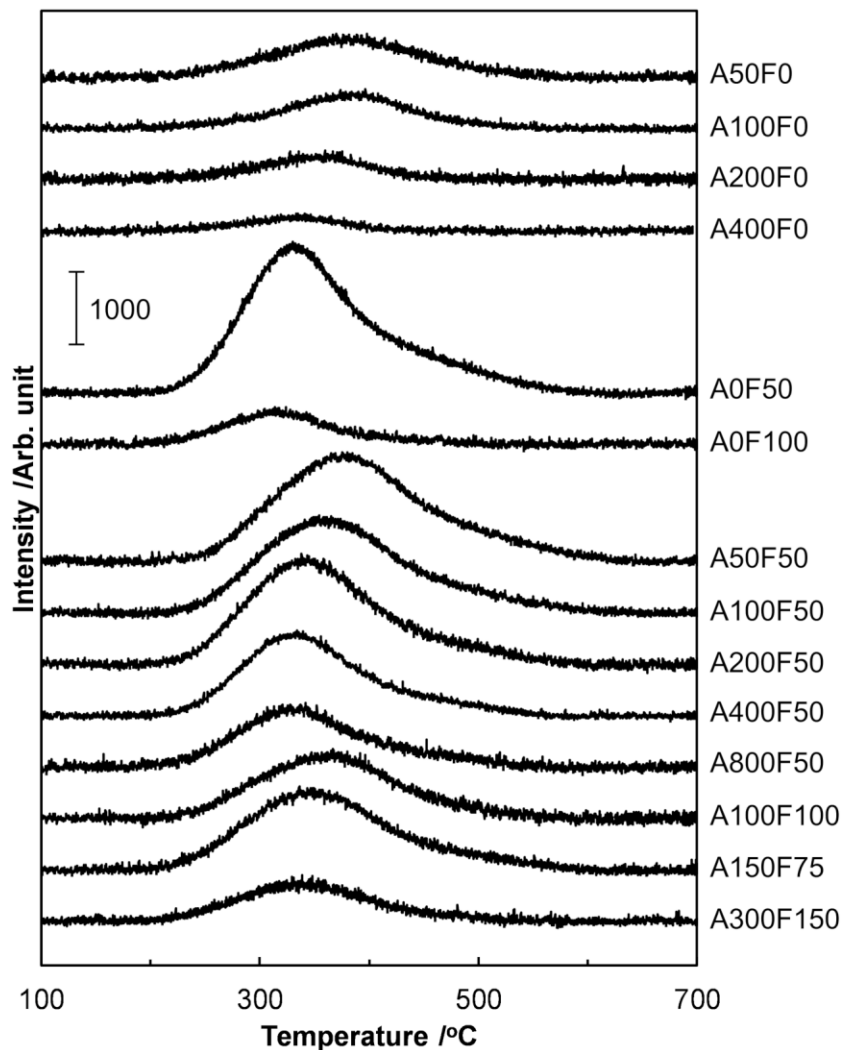


**Fig. S4** NH<sub>3</sub>-TPD profiles of the synthesized MFI zeolites, recorded by Q-MS at  $m/z = 16$ . These data were recorded after the surface saturation by NH<sub>3</sub> and the subsequent water-vapor treatment at 100 °C to remove the weakly-adsorbed NH<sub>3</sub> species.<sup>S1</sup>

The enthalpy change upon NH<sub>3</sub> desorption ( $\Delta H_{\text{NH}_3}$ ) was calculated from Fig. S4 and Eq. S1.<sup>S2</sup>

$$\ln T_m - \ln \left( \frac{A_0 W}{F} \right) = \frac{\Delta H_{\text{NH}_3}}{RT_m} + \ln \left( \frac{\beta (1 - \theta_m)^2 (\Delta H_{\text{NH}_3} - RT_m)}{p_0 e^{\frac{\Delta S_{\text{NH}_3}}{R}}} \right) \quad (\text{S1})$$

Here,  $T_m$  is the NH<sub>3</sub>-desorption temperature (unit: K),  $A_0$  is the acid density (mol kg<sup>-1</sup>),  $W$  is the sample amount (kg),  $F$  is the gas flow rate ( $= 1.0 \times 10^{-6} \text{ m}^3 \text{ s}^{-1}$ ),  $R$  is the gas constant ( $= 8.314 \text{ J K}^{-1} \text{ mol}^{-1}$ ),  $\beta$  is the temperature ramp rate ( $= 0.1667 \text{ K s}^{-1}$ ),  $\theta_m$  is the coverage of acid sites by NH<sub>3</sub> (dimensionless number),  $p_0$  is the standard pressure ( $= 1.0 \times 10^5 \text{ Pa}$ ), and  $\Delta S_{\text{NH}_3}$  is the entropy change upon NH<sub>3</sub> desorption ( $= 150 \text{ J K}^{-1}$ ).

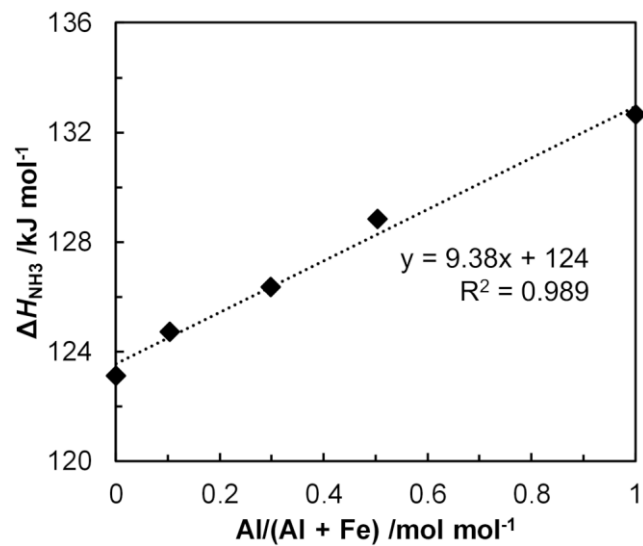


**Fig. S5** Parametric plot of the apparent  $\Delta H_{\text{NH}_3}$  for physical mixture of A50F0 and A0F50 at the different mixing ratios as a function of the proportion of Al in the total amount of Al and Fe. The values of  $\Delta H_{\text{NH}_3}$  were estimated by following the previously reported procedure (*vide supra*).<sup>S2</sup>

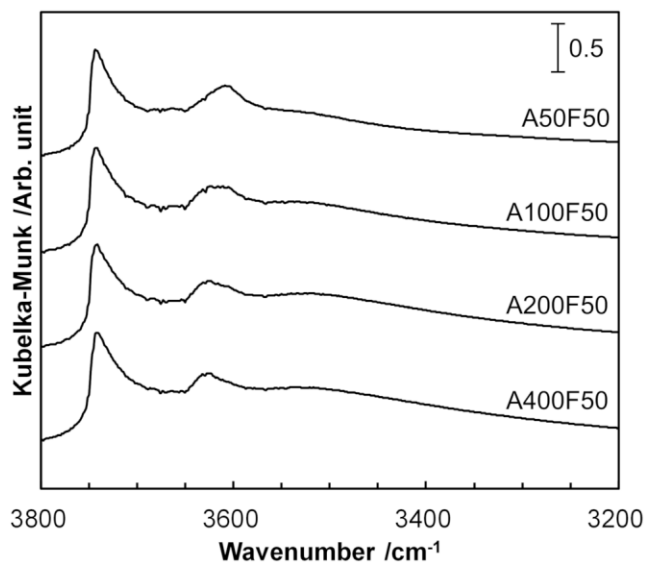


**Fig. S6** DRIFT spectra of the [Al, Fe]-MFI zeolites.

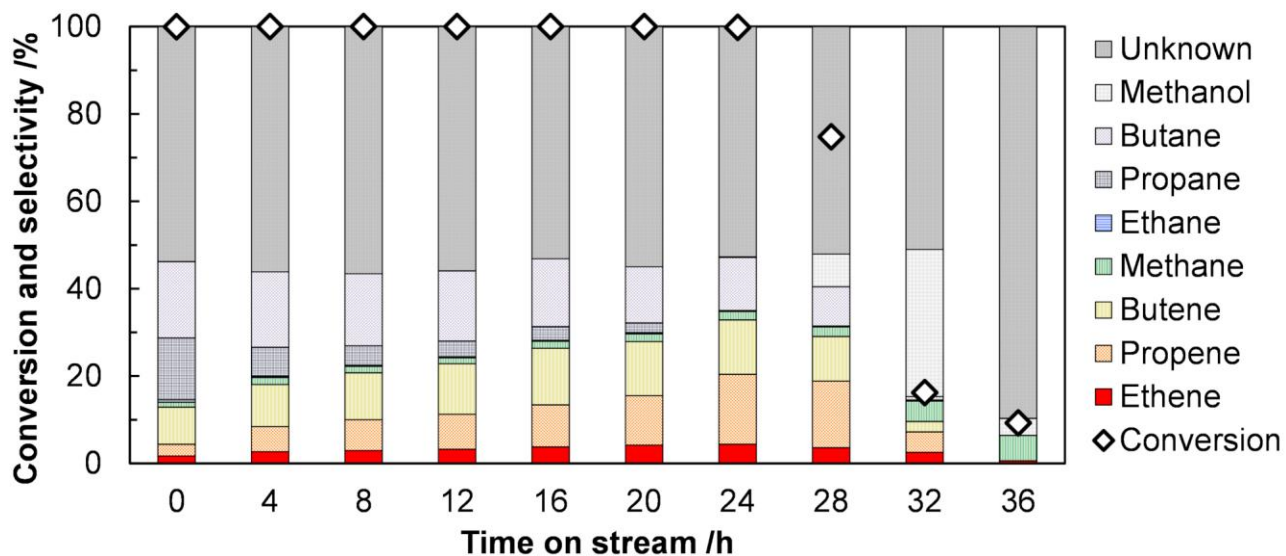


**Fig. S7** Detailed data of the DTO reaction using A50F0. Reaction conditions: A50F0 200 mg (mixed with 840 mg of quartz sand); 450 °C;  $W/F = 5.8 \text{ g h mol}^{-1}$ .

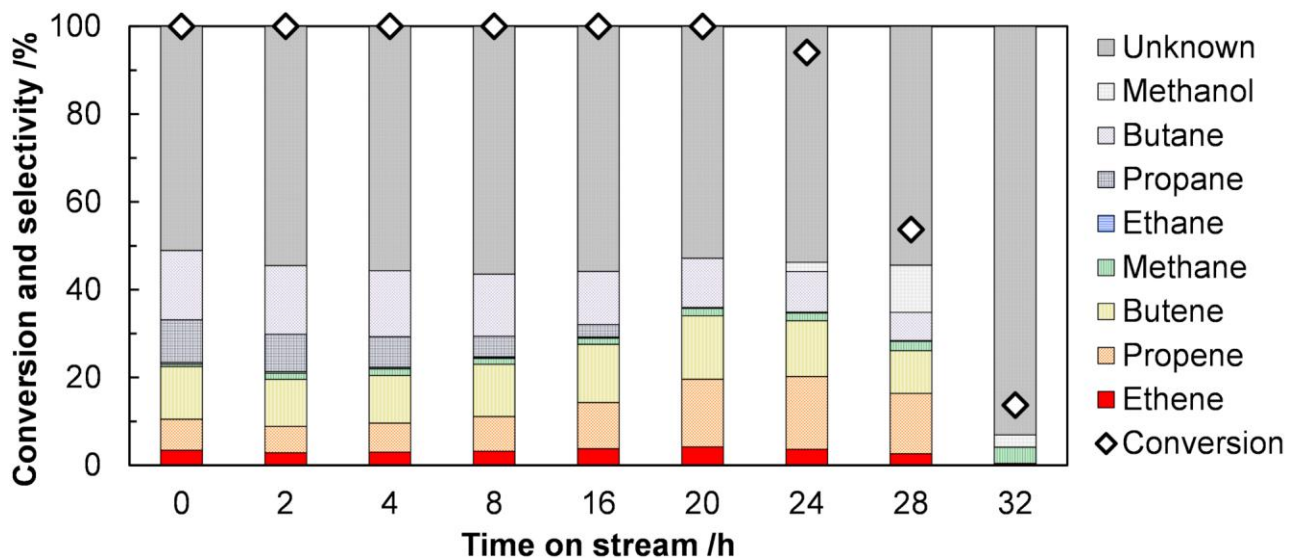


**Fig. S8** Detailed data of the DTO reaction using A100F0. Reaction conditions: A100F0 200 mg (mixed with 840 mg of quartz sand); 450 °C;  $W/F = 5.8 \text{ g h mol}^{-1}$ .



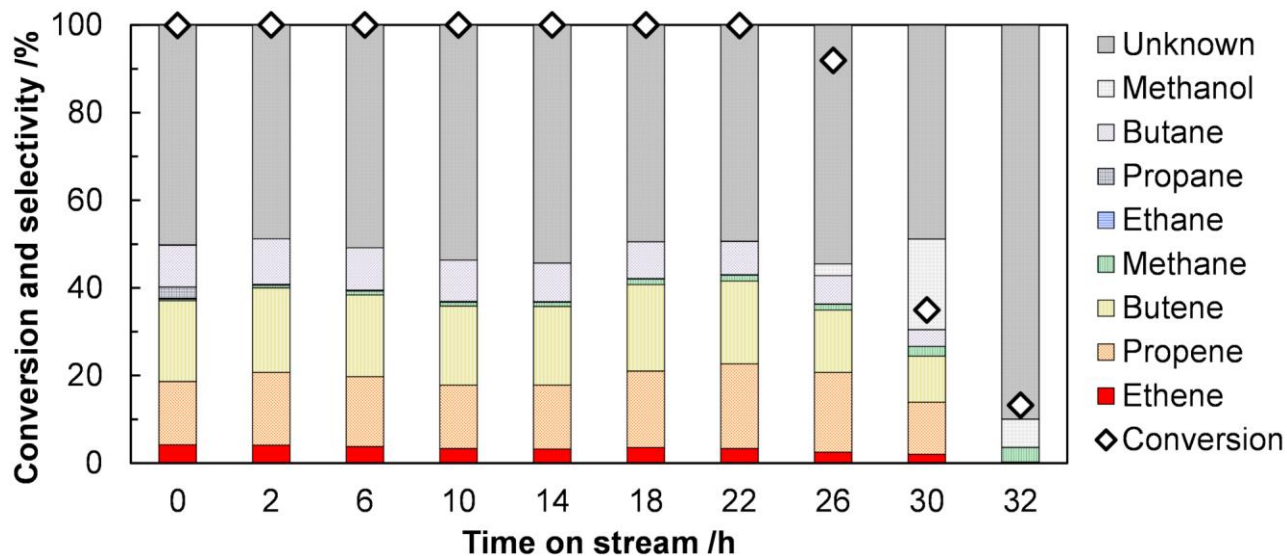


**Fig. S9** Detailed data of the DTO reaction using A200F0. Reaction conditions: A200F0 200 mg (mixed with 840 mg of quartz sand); 450 °C;  $W/F = 5.8 \text{ g h mol}^{-1}$ .

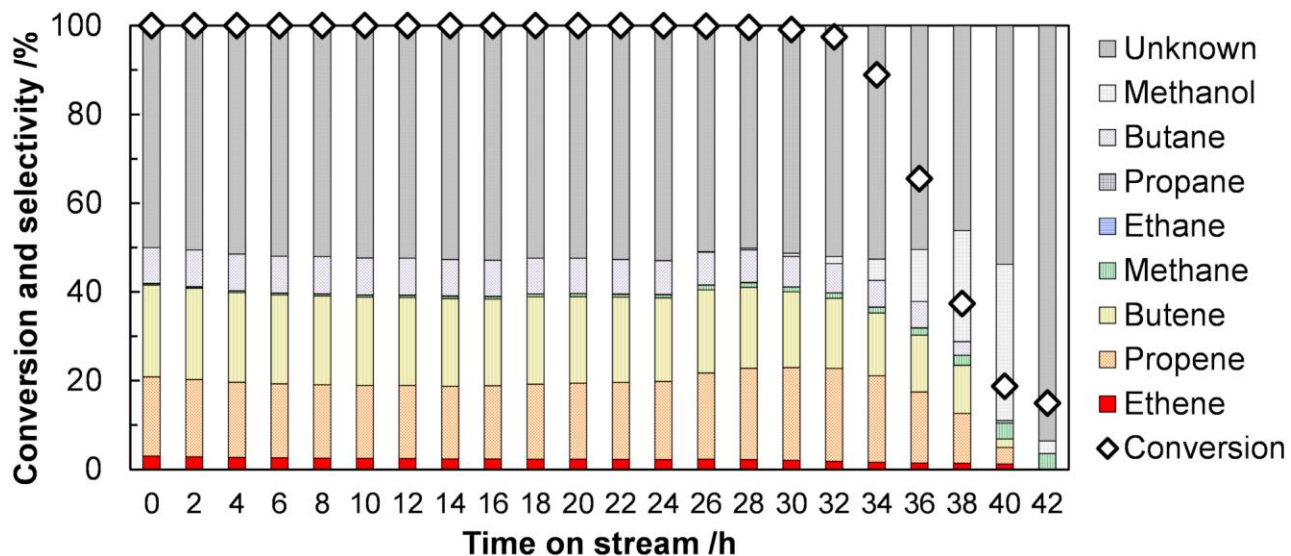


**Fig. S10** Detailed data of the DTO reaction using A400F0. Reaction conditions: A400F0 200 mg (mixed with 840 mg of quartz sand); 450 °C;  $W/F = 5.8 \text{ g h mol}^{-1}$ .

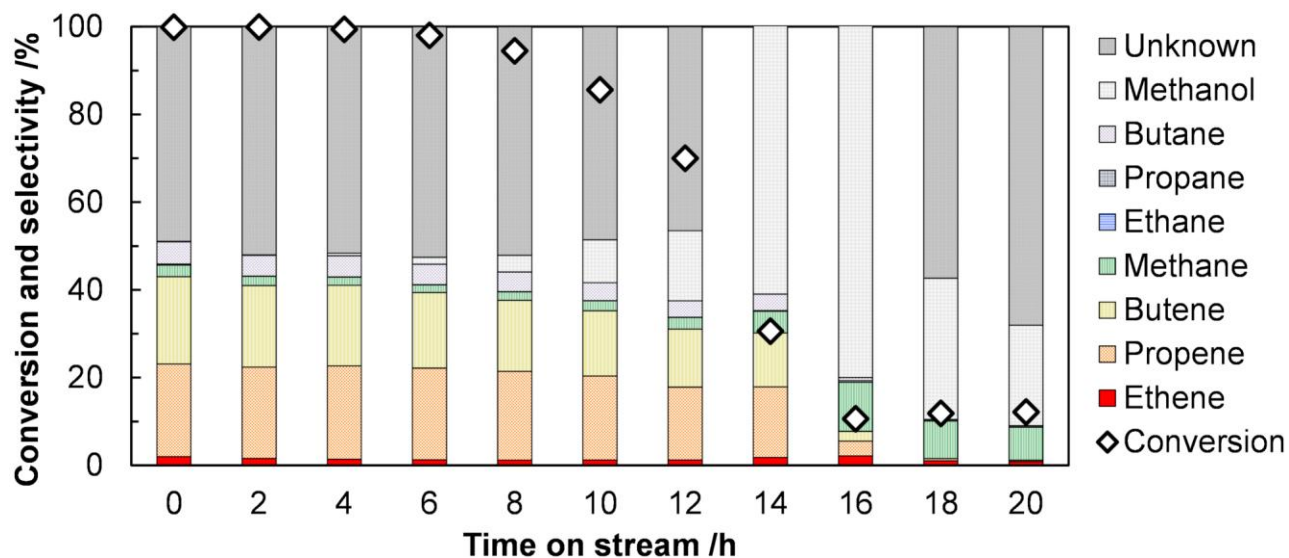


**Fig. S11** Detailed data of the DTO reaction using A0F50. Reaction conditions: A0F50 200 mg (mixed with 840 mg of quartz sand); 450 °C;  $W/F = 5.8 \text{ g h mol}^{-1}$ .

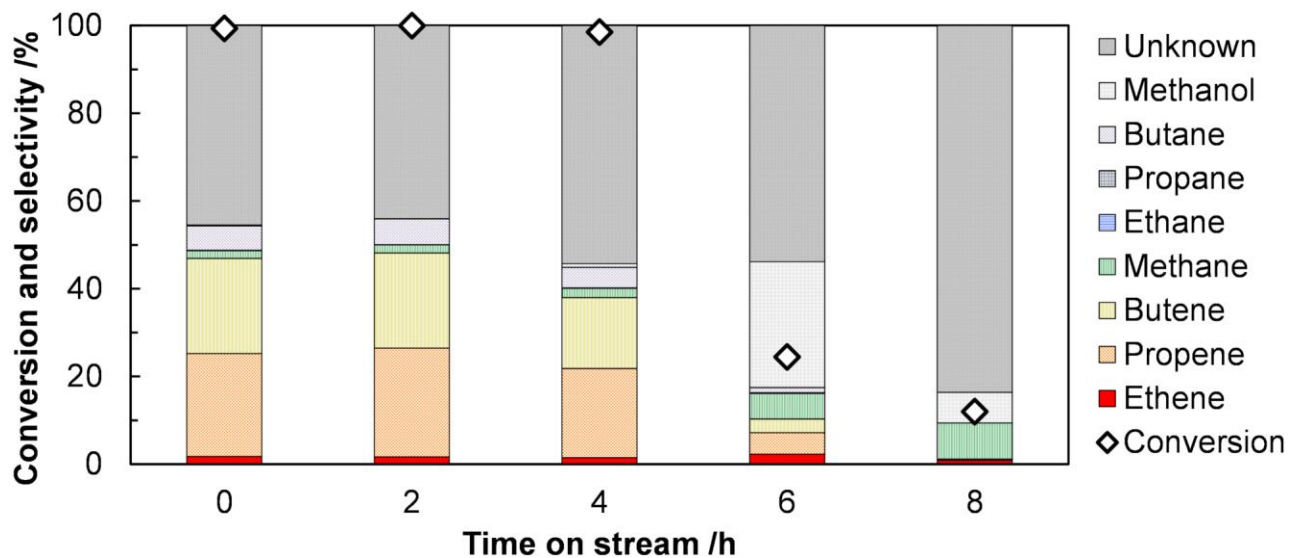


**Fig. S12** Detailed data of the DTO reaction using A0F100. Reaction conditions: A0F100 200 mg (mixed with 840 mg of quartz sand); 450 °C;  $W/F = 5.8 \text{ g h mol}^{-1}$ .

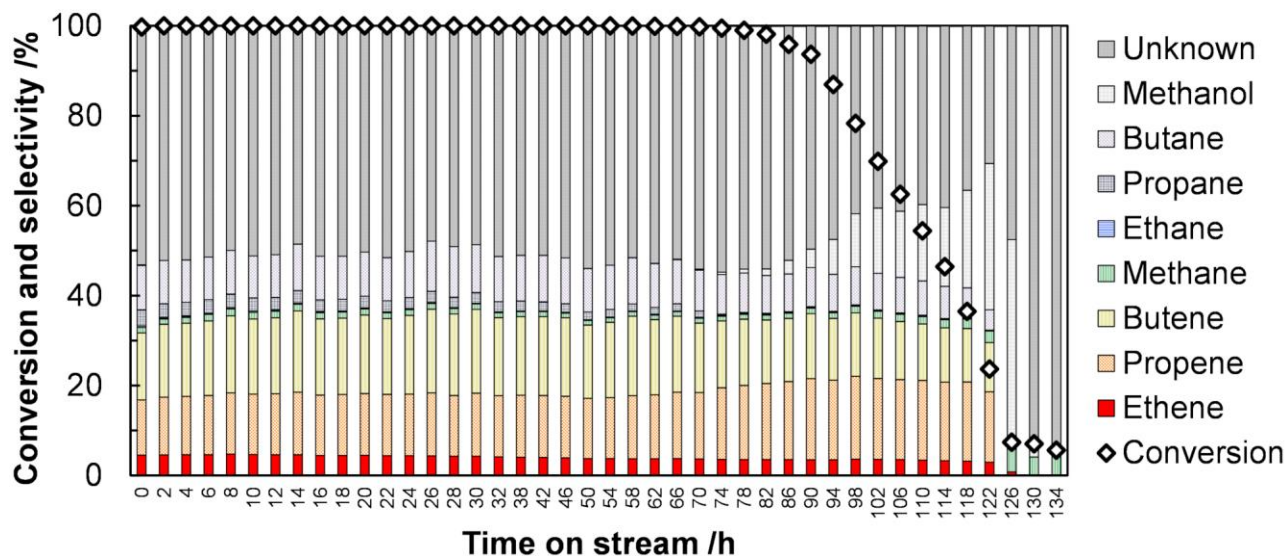


**Fig. S13** Detailed data of the DTO reaction using A50F50. Reaction conditions: A50F50 200 mg (mixed with 840 mg of quartz sand); 450 °C;  $W/F = 5.8 \text{ g h mol}^{-1}$ .

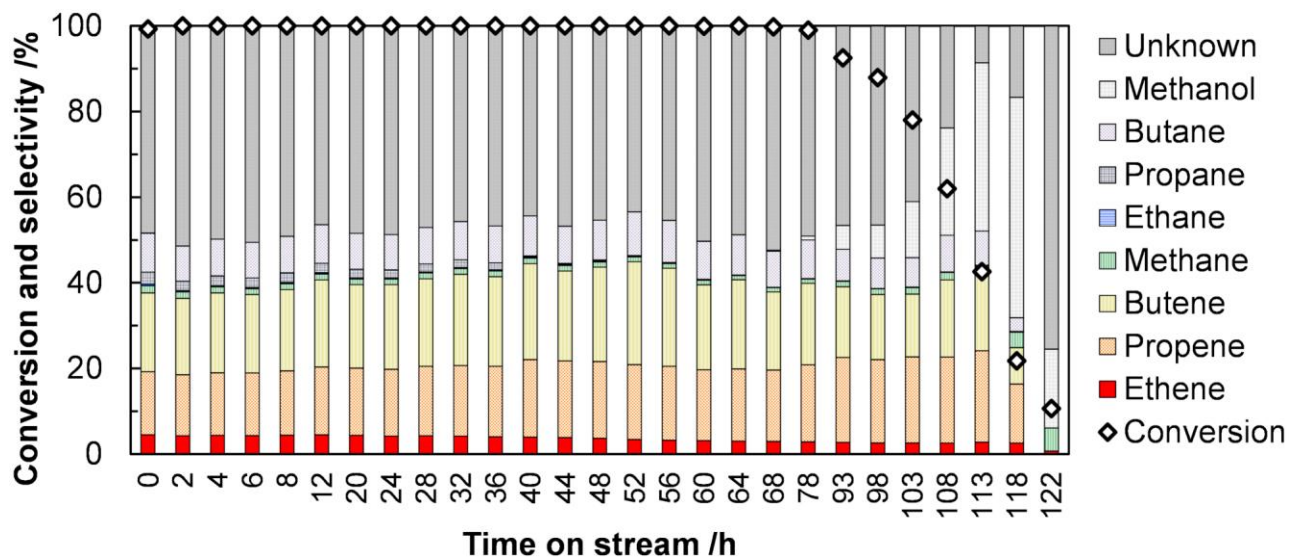


**Fig. S14** Detailed data of the DTO reaction using A100F50. Reaction conditions: A100F50 200 mg (mixed with 840 mg of quartz sand); 450 °C;  $W/F = 5.8 \text{ g h mol}^{-1}$ .

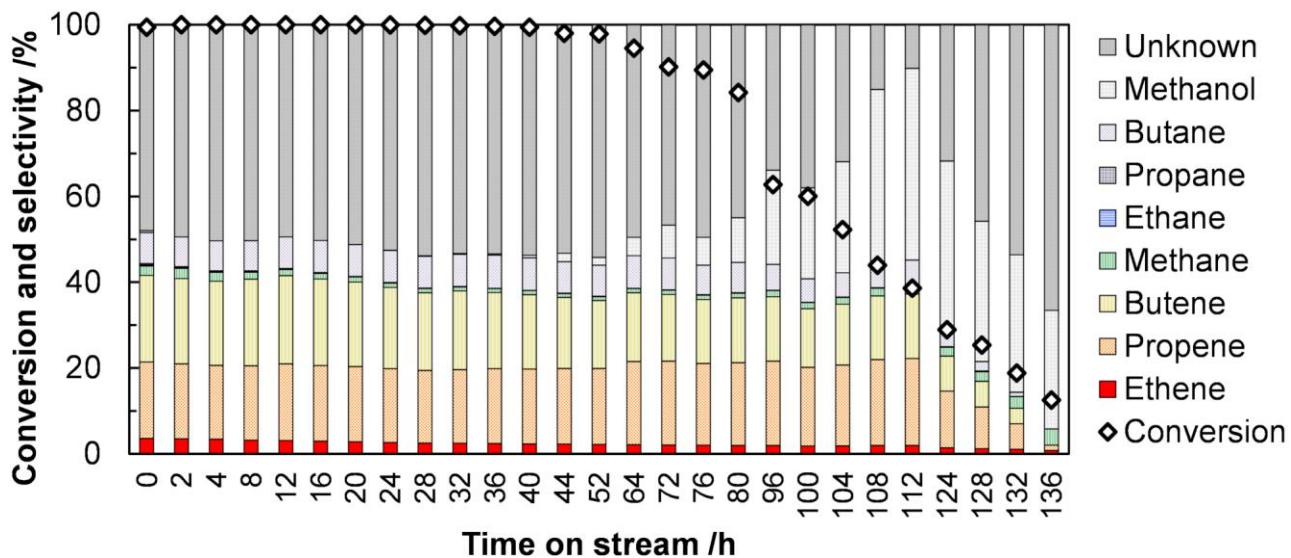


**Fig. S15** Detailed data of the DTO reaction using A200F50. Reaction conditions: A200F50 200 mg (mixed with 840 mg of quartz sand); 450 °C;  $W/F = 5.8 \text{ g h mol}^{-1}$ .

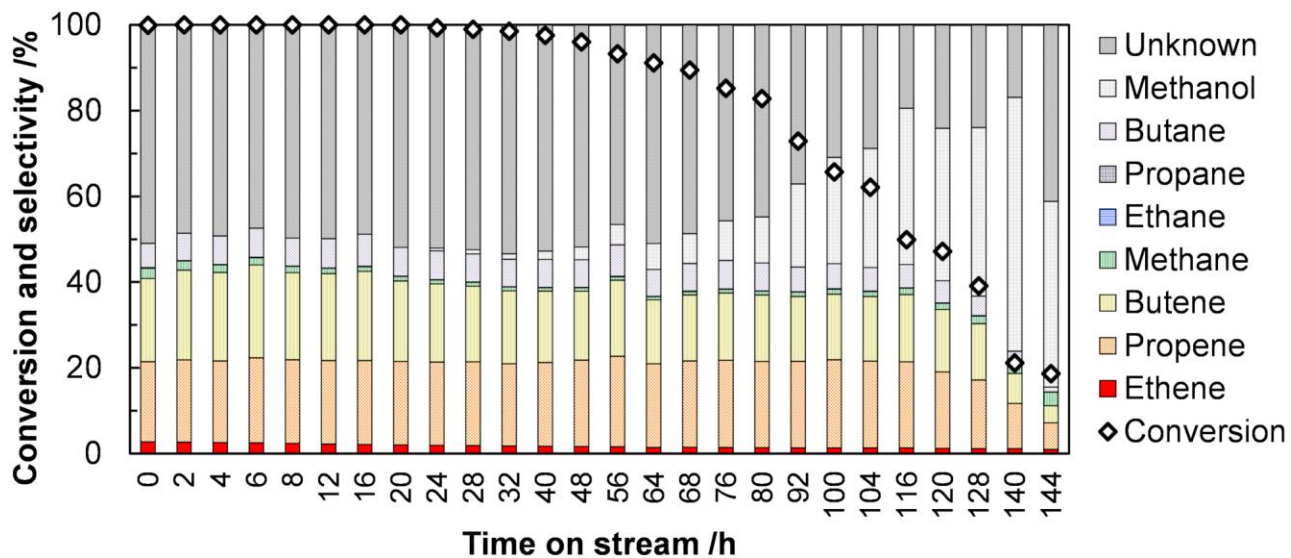


**Fig. S16** Detailed data of the DTO reaction using A400F50. Reaction conditions: A400F50 200 mg (mixed with 840 mg of quartz sand); 450 °C;  $W/F = 5.8 \text{ g h mol}^{-1}$ .

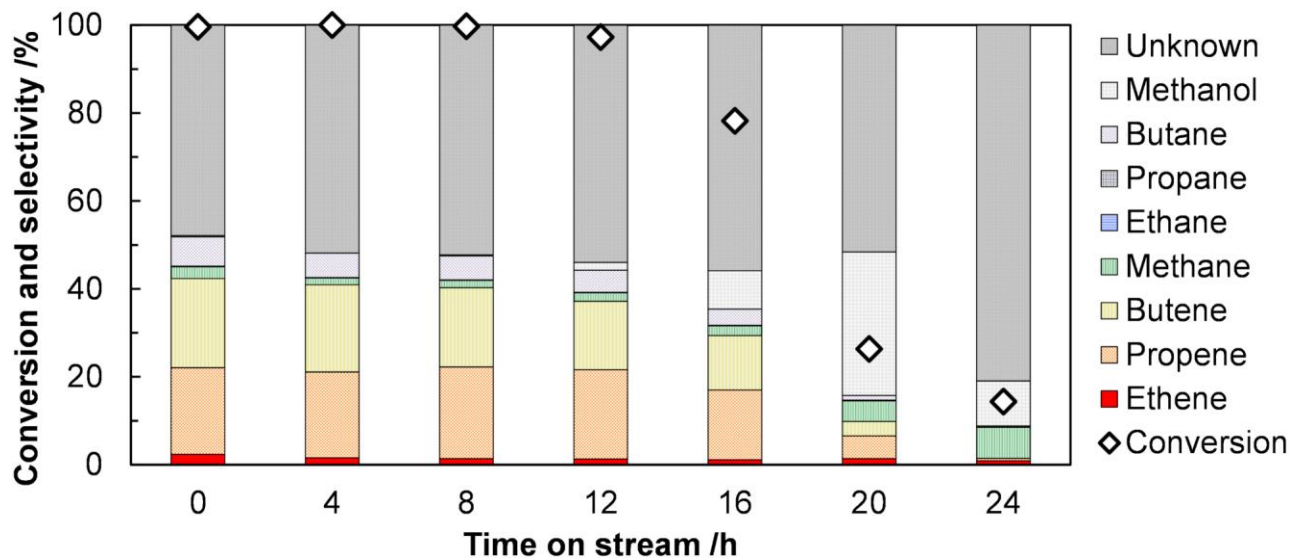


**Fig. S17** Detailed data of the DTO reaction using A800F50. Reaction conditions: A800F50 200 mg (mixed with 840 mg of quartz sand); 450 °C;  $W/F = 5.8 \text{ g h mol}^{-1}$ .

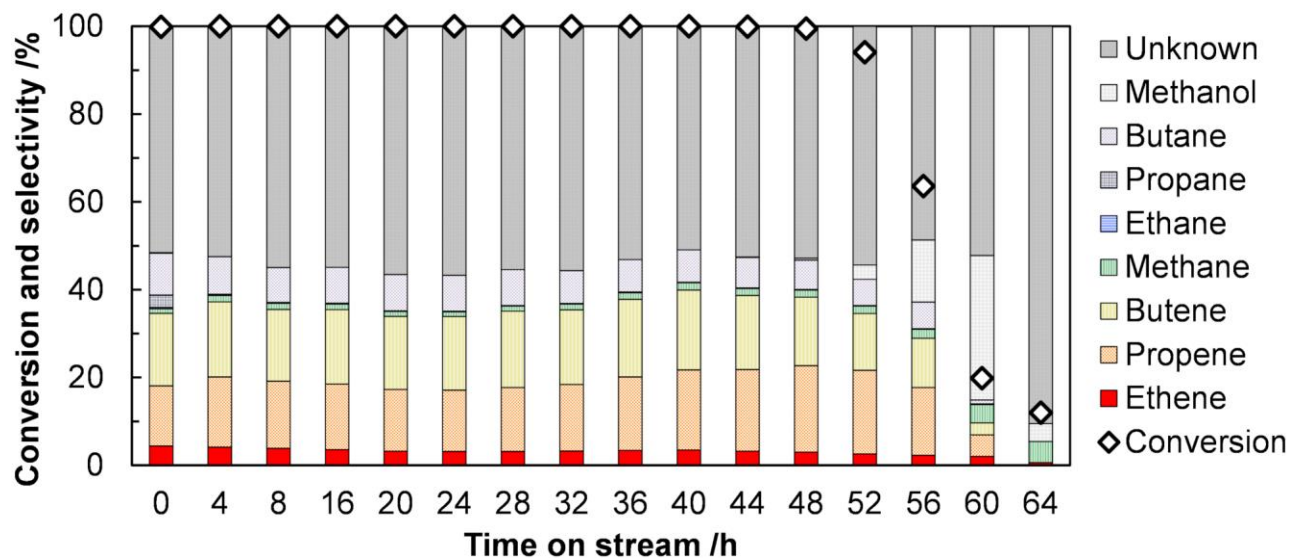


**Fig. S18** Detailed data of the DTO reaction using A100F100. Reaction conditions: A100F100 200 mg (mixed with 840 mg of quartz sand); 450 °C;  $W/F = 5.8 \text{ g h mol}^{-1}$ .

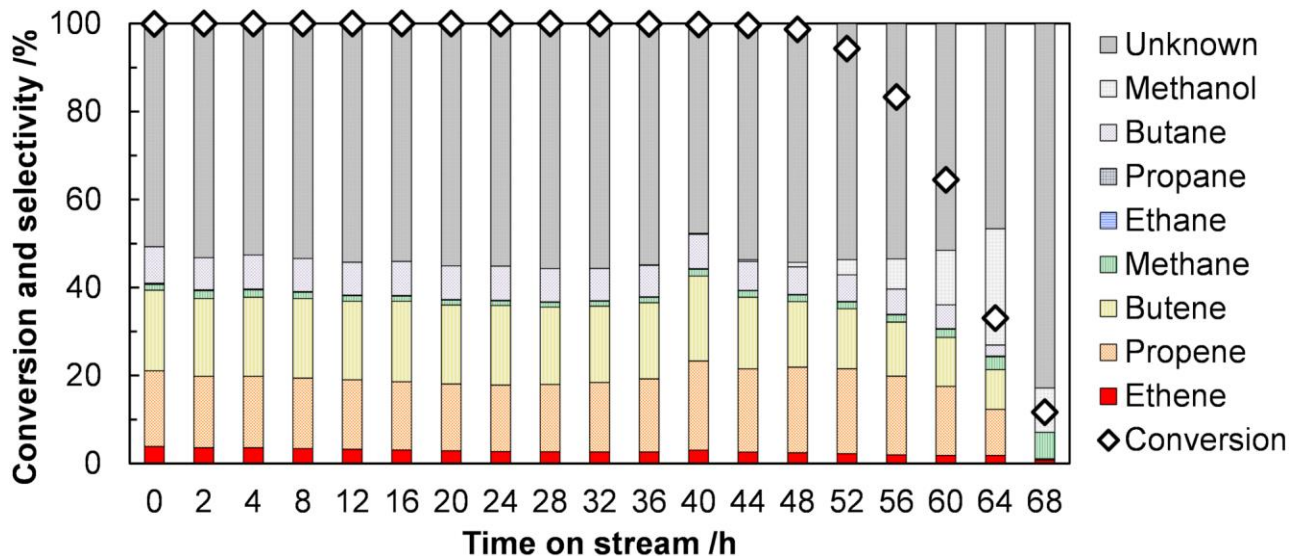


**Fig. S19** Detailed data of the DTO reaction using A150F75. Reaction conditions: A150F75 200 mg (mixed with 840 mg of quartz sand); 450 °C;  $W/F = 5.8 \text{ g h mol}^{-1}$ .

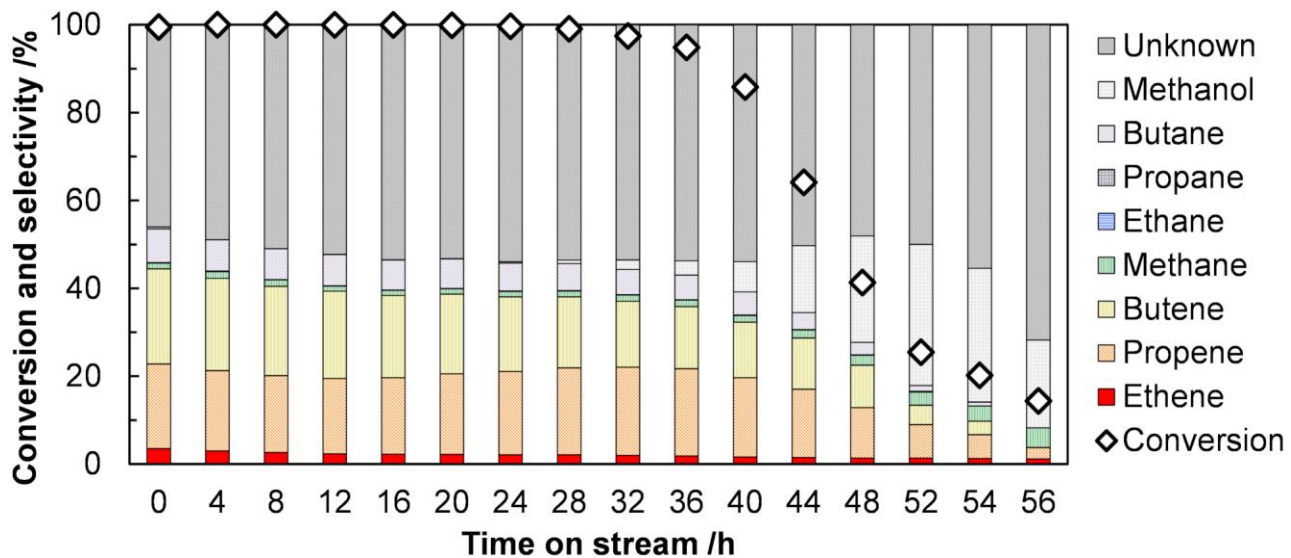


**Fig. S20** Detailed data of the DTO reaction using A300F150. Reaction conditions: A300F150 200 mg (mixed with 840 mg of quartz sand); 450 °C;  $W/F = 5.8 \text{ g h mol}^{-1}$ .

**Table S1** Ratios of propene to ethene produced in the DTO reaction

Catalyst	Ratio of propene to ethene <sup>a</sup>
A50F0	2.7
A100F0	3.1
A200F0	4.8
A400F0	8.0
A0F50	15
A0F100	14
A50F50	3.7
A100F50	4.9
A200F50	7.5
A400F50	11
A800F50	13
A100F100	5.0
A150F75	6.2
A300F150	8.6

<sup>a</sup> The value was calculated by averaging the data at the conversion of >50%.

**Table S2** Reported catalysts for the DTO reaction

Catalyst	Temp. /°C	GHSV or $W/F^a$	DME conv. /%	Light olefin selec. /%	Lifetime <sup>b</sup> /h	Ref.
H <sub>3</sub> PO <sub>4</sub> /12.5 wt% ZrO <sub>2</sub> / H-ZSM-5 (Si/Al = 42)	450	10 g h mol <sup>-1</sup>	100	63.1	N/A <sup>c</sup>	S3
SAPO-34 <sup>d</sup>	450	2.85 h <sup>-1 e</sup>	100	80–90	15	S4
CeO <sub>2</sub> -modified Ca-MFI (Si/Al = 100, Ca/Si = 0.025)	530	9.52 h <sup>-1 e</sup>	>99	45 <sup>f</sup>	250	S5
H-ZSM-5, partially ion-exchanged with Ca (Si/Al = 350)	530	1000 h <sup>-1</sup>	100	63.9	146 <sup>c</sup>	S6
11 wt% SAPO-34/ZrO <sub>2</sub>	400	3.54 h <sup>-1 e</sup>	100	80.5	470	S7
SAPO-34	460	0.72 h <sup>-1</sup>	99.8	78.8	7	S8
Phosphate-loaded MCM-68 (Si/Al = 60)	400	10.0 g h mol <sup>-1</sup>	96.7	69.8	N/A <sup>g</sup>	S9
CeO <sub>2</sub> -modified dealuminated MCM-68 (Si/Al = 110)	400	20 g h mol <sup>-1</sup>	>99	70	N/A <sup>g</sup>	S10
Mixture of RHO and SAPO-34 <sup>h</sup>	400	3000 mL g <sup>-1</sup> h <sup>-1</sup>	>99	90.2	6.3	S11
Hierarchical SAPO-34 (Si/Al = 0.18, Si/P = 0.23)	400	3 h <sup>-1 e</sup>	>99	80 <sup>i</sup>	7.9	S12
Nano-sized hierarchical ZSM-5 (Si/Al = 36)	400	1.8 h <sup>-1</sup>	>99	50.3	110 <sup>j</sup>	S13

<sup>a</sup> Gas hourly space velocity (GHSV, unit: h<sup>-1</sup>) or contact time ( $W/F$ , unit: g h mol<sup>-1</sup>). <sup>b</sup> The lifetime was defined as the time when the DME conversion became below 50%, unless otherwise noted. <sup>c</sup> At least 30 h. <sup>d</sup> Fluidized-bed reactor. <sup>e</sup> Weight hourly space velocity (WHSV). <sup>f</sup> Propene selectivity. <sup>g</sup> At least 5 h. <sup>h</sup> The DTO reaction was operated under the pressurized conditions (1.5 MPa). <sup>i</sup> Ethene and propene. <sup>j</sup> The lifetime was defined as the time when the conversion was 100%.



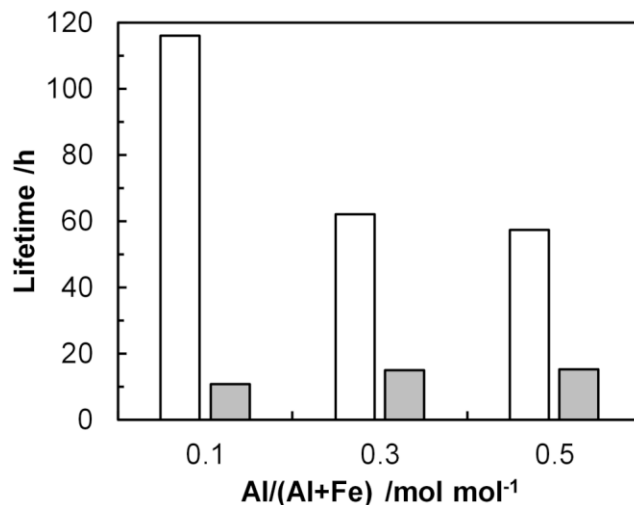


**Fig. S21** Differences of catalyst lifetime in the DTO reactions between [Al, Fe]-MFI (white bars) and a physical mixture of A50F0 and A0F50 (gray bars) at the various Al/(Al + Fe) values. Catalyst lifetime is defined as the time when the DME conversion becomes lower than 50%. Reaction conditions: catalyst 200 mg (mixed with 840 mg of quartz sand); 450 °C;  $W/F = 5.8 \text{ g h mol}^{-1}$ .

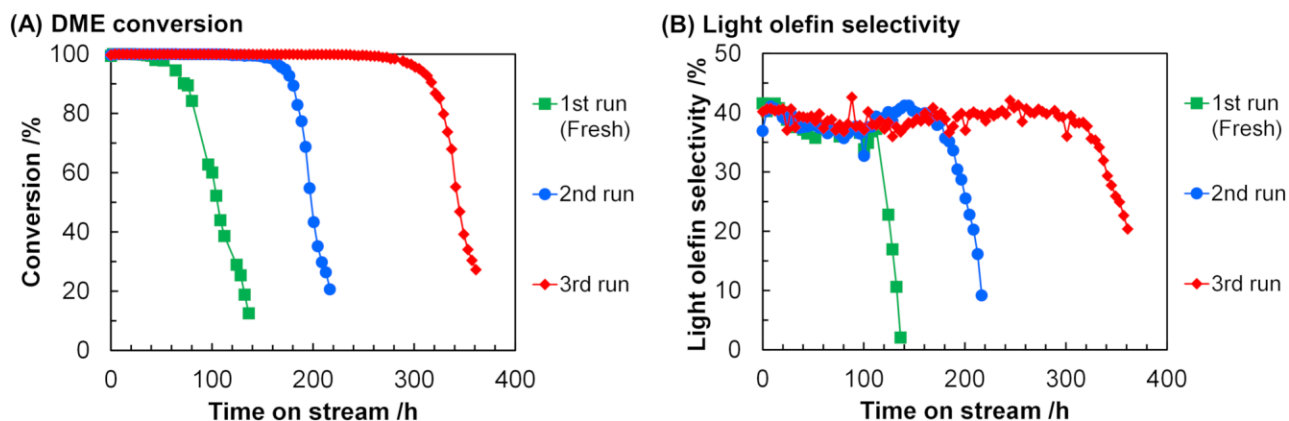


**Fig. S22** Recycle test of A200F50 for the DTO reaction. Before the second and third run, the catalyst was regenerated via calcination at 550 °C for 6 h in air. The data of the first run is the same as the one shown in Fig. 5. Reaction conditions: catalyst 200 mg (mixed with 840 mg of quartz sand); 450 °C;  $W/F = 5.8 \text{ g h mol}^{-1}$ .

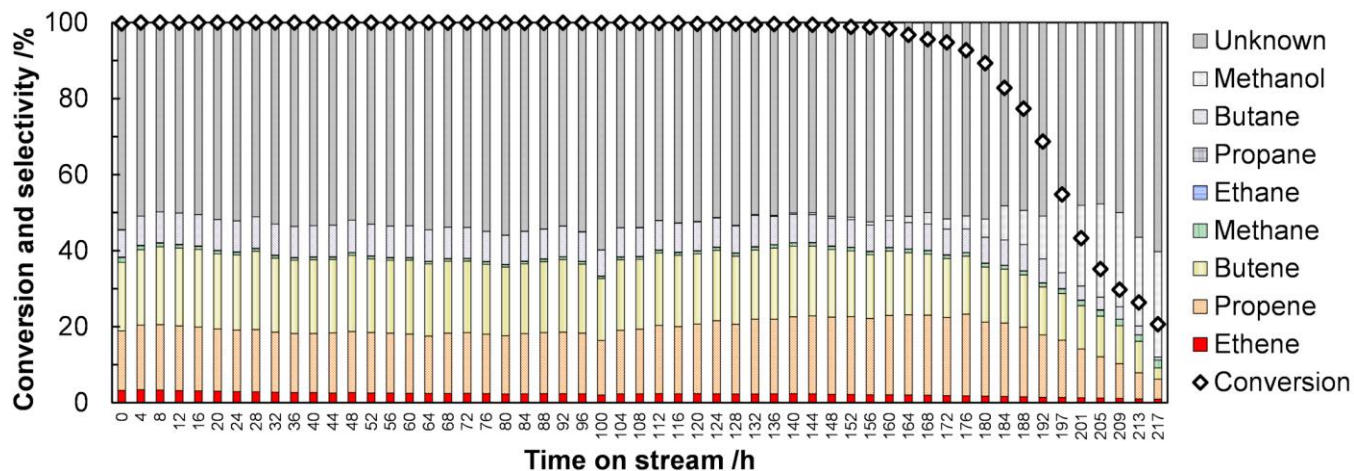


**Fig. S23** Detailed data of the second run of the DTO reaction using A200F50. Reaction conditions: A200F50 200 mg (mixed with 840 mg of quartz sand); 450 °C;  $W/F = 5.8 \text{ g h mol}^{-1}$ .

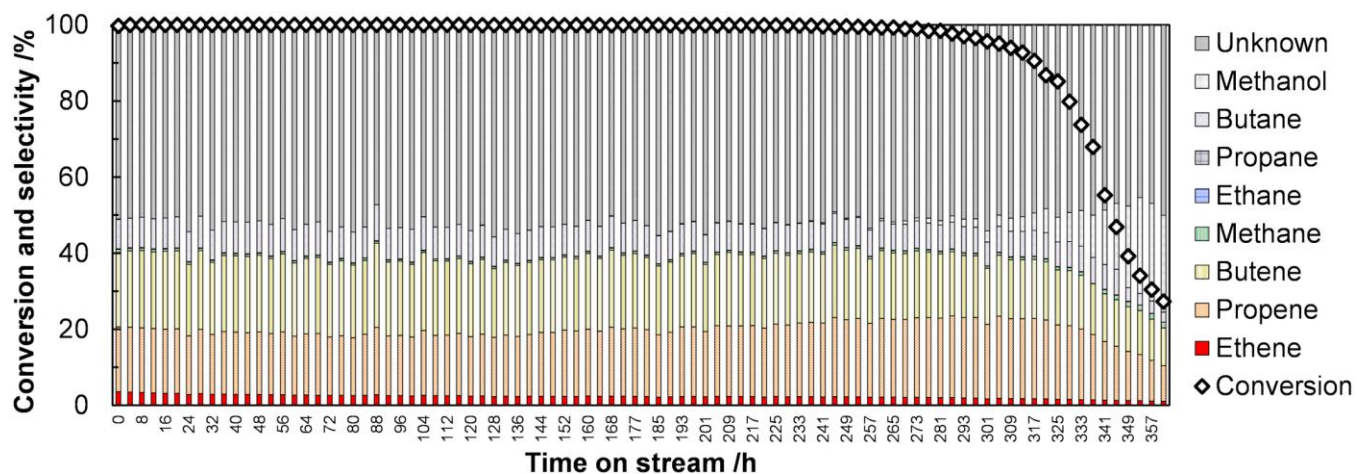


**Fig. S24** Detailed data of the third run of the DTO reaction using A200F50. Reaction conditions: A200F50 200 mg (mixed with 840 mg of quartz sand); 450 °C;  $W/F = 5.8 \text{ g h mol}^{-1}$ .

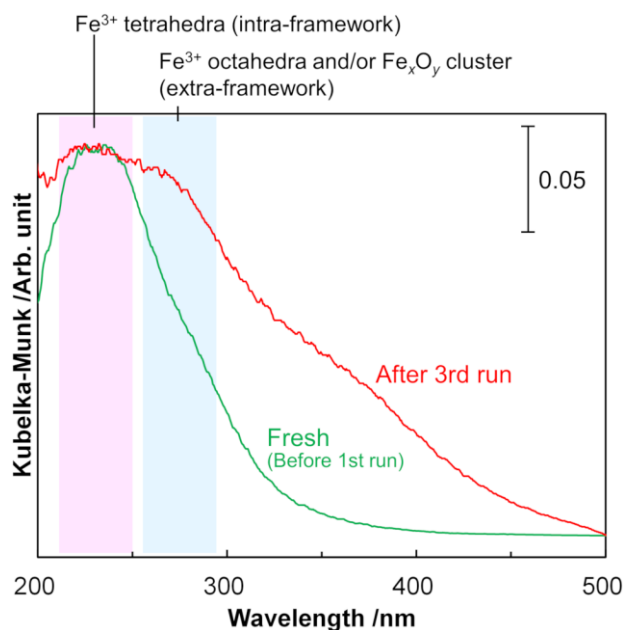


**Fig. S25** Differences of the nature of Fe species involved in the fresh A200F50 catalyst and the one after the third run of recycle test.

### Supplementary references

- S1 G. Bagnasco, *J. Catal.*, 1996, **159**, 249–252.
- S2 M. Niwa, N. Katada, M. Sawa and Y. Murakami, *J. Phys. Chem.*, 1995, **99**, 8812–8816.
- S3 T.-S. Zhao, T. Takemoto and N. Tsubaki, *Catal. Commun.*, 2006, **7**, 647–650.
- S4 Y. Chen, H. Zhou, J. Zhu, Q. Zhang, Y. Wang, D. Wang and F. Wei, *Catal. Lett.*, 2008, **124**, 297–303.
- S5 A. Iida, R. Nakamura, K. Komura and Y. Sugi, *Chem. Lett.*, 2008, **37**, 494–495.
- S6 K. Omata, Y. Yamazaki, Y. Watanabe, K. Kodama and M. Yamada, *Ind. Eng. Chem. Res.*, 2009, **48**, 6256–6261.
- S7 S.-G. Lee, H.-S. Kim, Y.-H. Kim, E.-J. Kang, D.-H. Lee and C.-S. Park, *J. Ind. Eng. Chem.*, 2014, **20**, 61–67.
- S8 M. Ghavipour, R. M. Behbahani, R. B. Rostami and A. S. Lemraski, *J. Nat. Gas Sci. Eng.*, 2014, **21**, 532–539.
- S9 S. Park, S. Inagaki and Y. Kubota, *Catal. Today*, 2016, **265**, 218–224.
- S10 Q. Han, K. Enoeda, S. Inagaki and Y. Kubota, *Chem. Lett.*, 2017, **46**, 1434–1437.
- S11 F. Wang, Z. Wen, Z. Qin, Q. Fang, Q. Ge, Z. Li, J. Sun and G. Li, *Fuel*, 2019, **244**, 104–109.
- S12 S. Zhang, Z. Wen, L. Yang, C. Duan, X. Lu, Y. Song, Q. Ge and Y. Fang, *Micropor. Mesopor. Mater.*, 2019, **274**, 220–226.
- S13 Z. Chen, Z. Li, Y. Zhang, D. Chevella, G. Li, Y. Chen, X. Guo, J. Liu and J. Yu, *Chem. Eng. J.*, 2020, **388**, 124322.